

Measurement and QCD Analysis of the e^+p Cross Section at HERA

A. Glazov
for the H1 Collaboration
DESY-Zeuthen, Platanenalle 6,
D-15738 Zeuthen, Germany



New measurements of the neutral current deep inelastic scattering (DIS) e^+p cross section performed by the H1 collaboration are discussed. The analysis of the structure function F_2 at low $2 < Q^2 < 100 \text{ GeV}^2$ leads to a determination of the gluon density based on data taken in 1995-1996. An extension of this analysis towards large $y < 0.86$ allowed a new determination of the longitudinal proton structure function F_L . Recently DIS cross section measurement was extended towards large $Q^2 \geq 5000 \text{ GeV}^2$ and high $x < 0.7$ based on about 37 pb^{-1} of luminosity collected in the years 1994-1997.

1 Introduction

The HERA collider operating with 27.5 GeV positrons and 820 GeV protons opened a new kinematic range in the measurements of the deep inelastic scattering cross section. The centre of mass energy of about $\sqrt{s} = 300 \text{ GeV}$ allowed to reach very high values of the momentum transfer squared Q^2 , up to 30000 GeV^2 at high Bjorken x , and very low x , of about 0.0001 at moderate $Q^2 \sim 10 \text{ GeV}^2$. The double differential cross section for the NC DIS reaction $e^+ + p \rightarrow e^+ + X$ is given by the following equation:

$$\frac{d^2\sigma}{dxdQ^2} = \frac{2\pi\alpha^2}{Q^4 x} Y_+ \left(F_2(x, Q^2) - \frac{y^2}{Y_+} F_L(x, Q^2) - \frac{Y_-}{Y_+} x F_3(x, Q^2) \right). \quad (1)$$

Here y denotes the inelasticity $y = Q^2/Sx$. Y_\pm is equal to $1 \pm (1 - y)^2$. F_2 , F_L and F_3 are generalized structure functions. The generalized structure function F_2 , for example, can be expressed as

$$F_2 = F_2^{em} + \frac{Q^2}{(Q^2 + M_Z^2)} F_2^{int} + \frac{Q^4}{(Q^2 + M_Z^2)^2} F_2^{wk} = F_2^{em}(1 + \delta_Z). \quad (2)$$

Here M_Z is the mass of the Z° and F_2^{em} , F_2^{wk} and F_2^{int} are the contributions to F_2 caused by photon exchange, Z° exchange and γZ° interference, respectively.

At low $Q^2 < 5000$ GeV 2 and low $y < 0.6$ the double differential cross section is dominated by F_2^{em} . Therefore the first structure function determined at HERA was the structure function $F_2(x, Q^2)$ ^{1,2,3,4}. Among various observations based on these data the most important ones are the steep rise of the structure function towards low x and the possibility to describe its Q^2 evolution within perturbative QCD down to $Q^2 \sim 1$ GeV 2 at low x .

At large $y > 0.6$ the contribution of the longitudinal structure function F_L to the DIS cross section becomes comparable to the one of F_2 . The H1 Collaboration thus developed a new method for the F_L determination. It was based on cross section measurements extended towards high y and on the assumption that the F_2 evolution is described by QCD⁵. The resulting structure function F_L was found to be large and within experimental errors consistent with the QCD prediction.

At high $Q^2 > 10000$ GeV 2 the electroweak effects become sizeable and all structure functions start to play a rôle. The very high Q^2 data is of special interest since the report of the H1 and ZEUS Collaborations of an excess of the number of observed events with respect to expectation of the standard model^{6,7}.

This paper presents new, preliminary results on the DIS cross section measurement obtained by the H1 collaboration. These are measurements of the DIS cross section at low $Q^2 < 100$ GeV 2 , based on data collected in 1995 – 1996⁸, and at high Q^2 based on data taken in 1994 – 1997.

The paper is organised as follows. Section 2 describes briefly the H1 detector. Section 3 explains the main methods used for the determination of the event kinematics. Section 4 highlights some aspects of the data analysis. Section 5 and 6 present the results obtained at low and high Q^2 , respectively. The conclusions and a brief discussion about future perspectives of the DIS cross section measurements at HERA are presented in Section 7.

2 The H1 Detector

The H1 detector⁹ is a nearly 4π hermetic apparatus with a solenoidal magnetic field of 1.15 T built to investigate high-energy ep interactions at HERA. In the low $Q^2 < 100$ GeV 2 region the scattered positron energy E'_e is measured in the backward electromagnetic lead-fibre calorimeter (SPACAL) which covers an angular range between 176° and 153°. Identification of the scattered positron and the polar angle measurement make use of a backward drift chamber (BDC) in front of the SPACAL. The interaction vertex is determined with the central drift chambers: the jet chamber CJC and the two z drift chambers.

The energy of the scattered positron in the high $Q^2 \geq 200$ GeV 2 analysis is reconstructed with the Liquid Argon (LAr) calorimeter which covers an angular region between 3° and 155°. The polar angle measurement is based on the tracking detectors.

The energies of the hadronic final state particles are reconstructed using the LAr and SPACAL calorimeters and also the central tracking detectors.

The luminosity is determined from the cross section of the elastic bremsstrahlung process, measured with a precision of 1.5%-2.6%. The final state photon and the positron scattered at very low Q^2 can be detected in calorimeters ("photon and electron taggers") which are situated close to the beam pipe at distances of 33 m and 103 m from the interaction point in the positron beam direction.

The use of the H1 detector for the inclusive DIS cross section measurement is further discussed in².

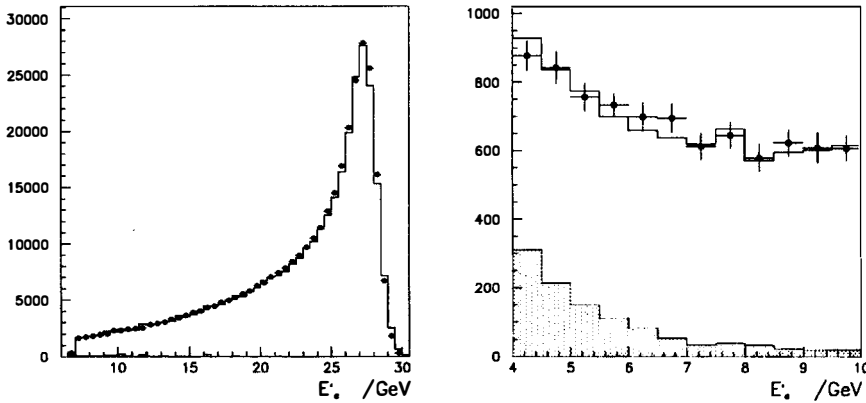


Figure 1: Distributions of the energy of the scattered positron for the low $Q^2 < 100$ GeV^2 data sample taken in 1996. The left figure corresponds to the standard F_2 analysis ($y < 0.7$). The right figure shows energy distributions for the dedicated high y analysis ($y < 0.86$). Solid points represent the data, the open histograms show the sum of DIS Monte Carlo expectation, based on the DJANGO¹⁰ program and the photoproduction background (shaded histograms). The latter was estimated using a PHOJET¹¹ simulation or using clusters linked to a negative track (see text)

3 Kinematics

A special feature of a collider experiment is the possibility to reconstruct the kinematics using both the positron and the hadronic final state particles. In the first case the event kinematics were reconstructed using the energy of the scattered lepton E'_e and the polar angle θ_e according to the relations

$$y_e = 1 - \frac{E'_e \sin^2 \theta_e}{2} \quad Q_e^2 = 4E'_e E_e \cos^2 \frac{\theta_e}{2} = \frac{E'^2_e \sin^2 \theta_e}{1 - y_e}. \quad (3)$$

Here θ_e is defined with respect to the proton beam direction, defining the z axis. This reconstruction method is called the 'electron (E)' method. It is best applicable at large values of y .

At low y the Σ method was used. This method combines the positron and the hadronic measurements by defining

$$y_\Sigma = \frac{\Sigma}{\Sigma + E'_e(1 - \cos \theta_e)} \quad Q_\Sigma^2 = \frac{E'^2_e \sin^2 \theta_e}{1 - y_\Sigma}, \quad (4)$$

with

$$\Sigma = \sum_h (E_h - P_{z,h}) \quad (5)$$

Here E_h and $P_{z,h}$ are the energy and longitudinal momentum component of a particle h , the summation is over all hadronic final state particles, and masses are neglected.

For the low Q^2 analysis the resulting DIS cross section measurement was split between E and Σ methods. At high $y > 0.15$ the electron method was used. In the high Q^2 analysis the kinematics was reconstructed using the combination of Q_e^2 and x_Σ in the whole kinematic range.

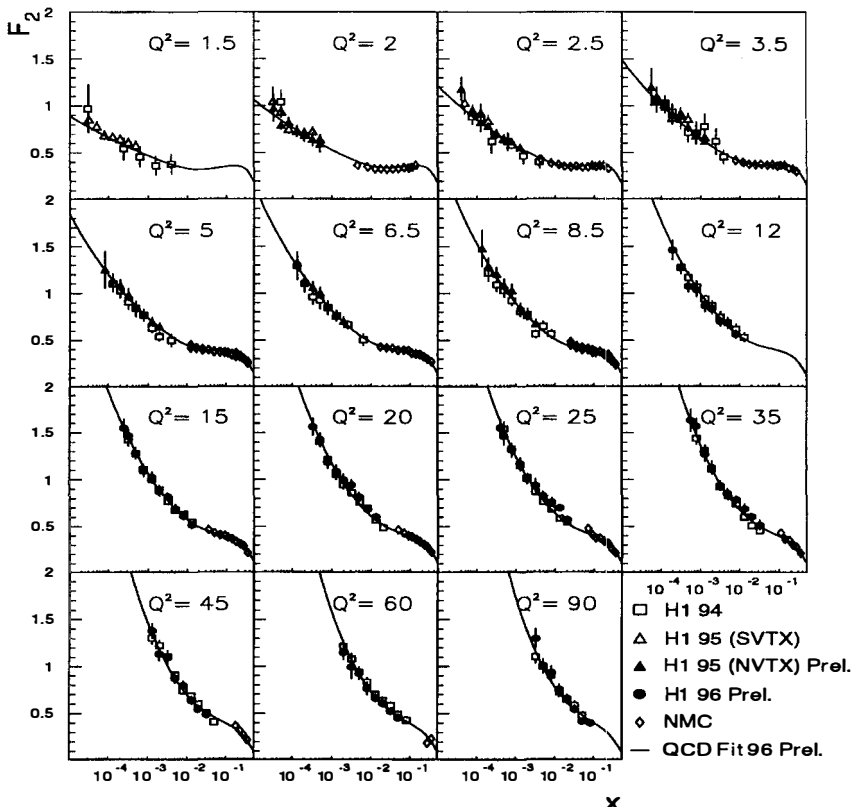


Figure 2: Determinations of the structure function $F_2(x, Q^2)$ by the H1 experiment. The new data (1995 data for Q^2 between 2 and 8.5 GeV^2 and 1996 data for Q^2 between 12 and 90 GeV^2) are in good agreement with the previous results on F_2 which used a different detector, apart from the 1995 shifted vertex data (SVTX)¹⁵. The curves represent the preliminary result of a NLO QCD fit to the H1, NMC and BCDMS structure function data.

4 Data Analysis

The new data presented here improves previous H1 results in the region $Q^2 < 10 \text{ GeV}^2$ and $Q^2 \geq 200 \text{ GeV}^2$ where systematic errors of 6% and 8% were reached, respectively.

One of the major sources of the systematic error is the uncertainty of the scattered positron energy. The calibration of the electromagnetic calorimeter was performed using the double angle method in which the event kinematics is reconstructed using the polar angles of the positron and of the hadronic final state particles. In the case of the high Q^2 analysis an uncertainty of 1% was achieved in the central region ($\theta_e > 80^\circ$) rising to 3% for smaller angles due to limited statistics. An example of the energy distribution in the case of low $Q^2 < 100 \text{ GeV}^2$ analysis is presented in Figure 1-left. A good description of the measured energy spectrum by the Monte Carlo simulation in the “kinematic peak” region, where the energy of the scattered positron is about the positron beam energy, proves the energy scale to be understood to better than 1%.

At high $y > 0.6$ the data analysis has to deal with several additional complications. One of these is an increase of the background from photoproduction events in which the scattered

positron escapes undetected in the beam pipe and a hadronic final state particle fakes the scattered positron candidate. In Figure 1-right one can see that at lowest energies the background contribution reaches about 30%. In order to reduce the uncertainty of the background estimation the high y cross section measurement was restricted to the acceptance of the central tracking chambers. The positron candidate was then required to be linked with a track in the CJC. Therefore the background could be estimated directly from the data using clusters associated with tracks of a wrong charge. The studies of the charge symmetry of the background and the charge resolution of CJC allowed to estimate the systematic error on the background contamination to be 3% of its amount.

Further details on the analysis of the DIS cross section can be found in ^{12,13,7}.

5 Results at Low $Q^2 < 100 \text{ GeV}^2$

5.1 The Proton Structure Function $F_2(x, Q^2)$

At low Q^2 and low y the DIS cross section is determined by the structure function $F_2(x, Q^2)$. Figure 2 presents the preliminary H1 data together with previous structure function measurements of H1 and higher x data of NMC ¹⁸. There is remarkable agreement of the new H1 data with the H1 1994 data although the latter has been taken with a different apparatus in the backward direction. Small departures between the two data sets are due to local systematic effects but are covered by the systematic errors assigned. The curves in Figure 2 represent a next-to-leading order QCD fit to the H1, NMC and BCDMS data which is used for a new determination of xg as described below. There is good agreement between the fit and the measurement over the whole kinematic range presented in the figure.

5.2 The Gluon Distribution $xg(x, Q^2)$

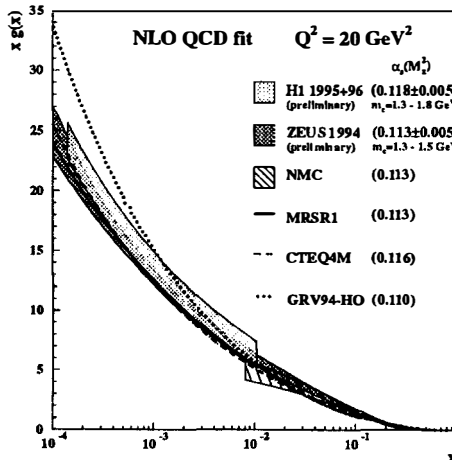


Figure 3: Gluon distributions resulting from NLO QCD analyses performed by the H1 and ZEUS collaborations. The error bands comprise the statistical and systematic errors and also the uncertainties due to α_s and the charm quark mass m_c .

The gluon distribution can be extracted from the scaling violations of the structure function F_2 . A QCD fit was performed in the \overline{MS} renormalisation scheme using the DGLAP evolution

equations¹⁷ for three light flavours with the charm contribution added using the NLO calculation of the photon-gluon fusion process^{18,20}. The numerical solution of the DGLAP equations used the procedure described in²¹. The input parton distributions $xg(x)$, $xu_v(x)$, $xd_v(x)$ and $xS(x)$ at the starting scale $Q_0^2 = 1 \text{ GeV}^2$ were parameterised using the functional form $xf_i = A_i x^{B_i} (1-x)^{C_i} (1 + D_i x + E_i \sqrt{x})$. D_g, E_g were taken to be zero and $S = \bar{u} = \bar{d} = 2\bar{s}$ defines the sea distributions. In order to reduce the influence of the longitudinal structure function on this fit a cut of $y < 0.6$ was used for all H1 data sets. The minimum y is approximately equal to 0.01 for all Q^2 values. Besides the H1 data the proton and deuterium data of the muon scattering experiments BCDMS²² and NMC¹⁶ were used to constrain the high x behaviour of the parton distributions.

A similar analysis was performed by the ZEUS collaboration²³. The resulting gluon distributions at $Q^2 = 20 \text{ GeV}^2$ as a function of x are shown in Figure 3. The gluon distribution rises towards low x . This can be explained by the asymptotic behaviour in $\ln 1/x$ of the solutions to the DGLAP equations.

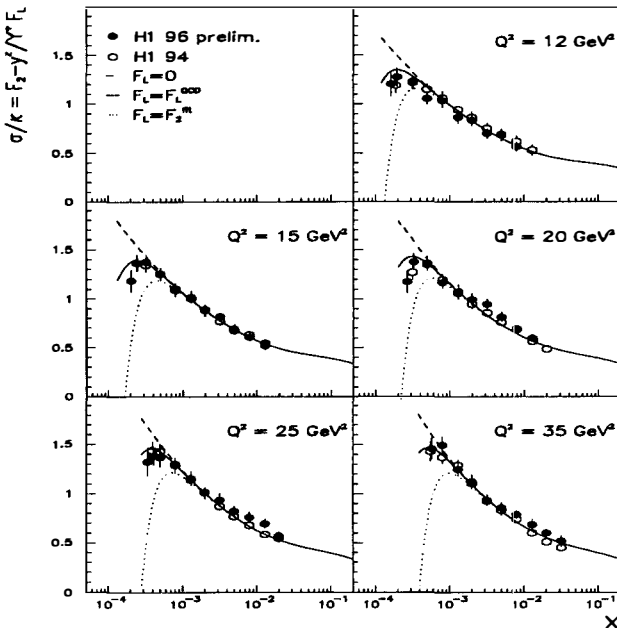


Figure 4: Measurement of the DIS cross section divided by the kinematic factor $\kappa = (2\pi\alpha^2 Y_+)/Q^4 x$. The curves use the QCD calculation of F_2 and F_L (full curve) or the extreme assumptions $F_L = F_2$ (dotted curve) and $F_L = 0$ (dashed curve). The largest central y values are 0.82. For $Q^2 \geq 35 \text{ GeV}^2$ this y range is outside the SPACAL acceptance.

The error bands of the gluon distributions include both systematic uncertainties and a possible variation of α_S by ± 0.005 and of the charm quark mass m_c by $\pm 0.3 \text{ GeV}$ ($\pm 0.1 \text{ GeV}$ in the case of the ZEUS analysis). There is good agreement between the H1 and the ZEUS gluon density determinations inside the quoted errors.

It is known that the determination of the gluon distribution using only charged lepton structure function data leads to a behaviour of xg at high x which differs from the results of

global analyses which include direct photon data²⁴. Therefore the H1 result in Figure 3 is given only for $x < 0.01$. Moreover, a control fit was done with a five parameter gluon distribution fixing the parameters which determine the high x behaviour of xg . This leads to a gluon distribution which is lower by nearly 10% at $x = 0.01$ but in very good agreement with the standard three parameter gluon at lower x . The difference of these two determinations has been included in the error band drawn in Figure 3. It is largely responsible for the error of xg at x near to 0.01. This source was not included into the error band of the ZEUS gluon determination.

5.3 The Cross Section at High y and the Structure Function $F_L(x, Q^2)$

The result on the measured DIS cross section for Q^2 between 12 and 35 GeV^2 is shown in Figure 4 comparing the 1994 data⁵ (open points) with the analysis of the 1996 data (closed points). The error bars comprise both statistical and systematic errors added in quadrature. Both cross section measurements agree well.

Figure 4 shows also calculations of the cross section using the QCD fit to F_2 and three different assumptions on the longitudinal structure function F_L . The measured cross section is in agreement with the NLO QCD calculation apart from large y , for $12 \leq Q^2 \leq 25 \text{ GeV}^2$, where the measured points tend to be lower than the QCD curves (solid curves in Figure 4).

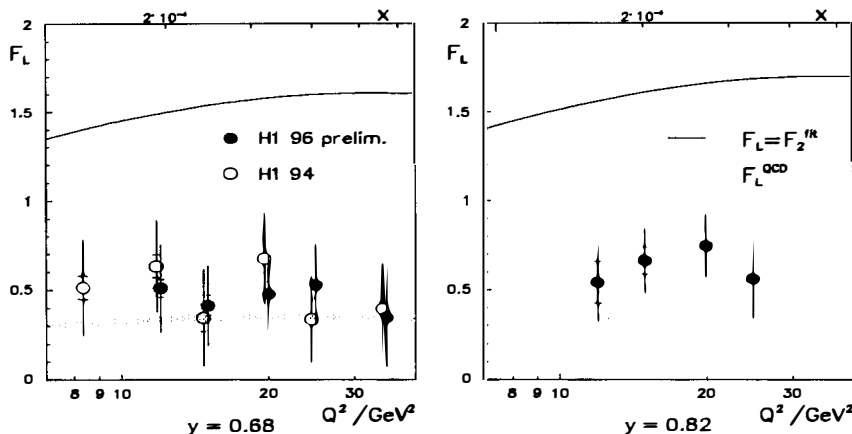


Figure 5: Determination of the longitudinal structure function $F_L(x, Q^2)$ as a function of Q^2 or $x = Q^2/sy$ for $y = 0.68$ and $y = 0.82$. The inner error bars are the statistical errors. The full error bars represent the statistical and systematic errors added in quadrature. The error bands represent the uncertainty of the F_L calculation. The upper lines define the allowed upper limit of $F_L = F_2$, where F_2 is given by the QCD fit.

The cross section measurement at high y can be converted to a determination of the longitudinal structure function $F_L(x, Q^2)$ assuming that F_2 in this region is given by the DGLAP equations in NLO using the H1 and fixed target data as was discussed in Ref. ⁵. In order to represent the cross section measurement as a determination of F_L , a QCD fit to the new H1 data (1995, 1996), for $y < 0.35$, and to the BCDMS and NMC data was performed and F_2 in the high y region of the H1 data was calculated. The result agrees within 2% with the former calculation of F_2 ⁵ which used the 1994 H1 data and the BCDMS data. The resulting F_L values are shown in Figure 5. For $y = 0.68$ the new result is in good agreement with the 1994 data (open points). The region of $y > 0.78$, i.e. of lowest x at fixed Q^2 , was not accessible prior to this analysis.

The data are compared with the calculation of F_L in NLO QCD (shaded band in Figure 5) using the fit described and the prescription of Ref.¹⁹ for three light flavours and of Ref.²⁰ for the charm contribution. This calculation agrees very well with the previous calculation, presented in Ref. 5, although it used different input distributions and programs. The experimental uncertainty of this calculation has improved to about 6%. Most of the data points are higher than the QCD expectation which is also visible in the cross section measurement at high y , Figure 4.

6 Results at High $Q^2 \geq 200 \text{ GeV}^2$

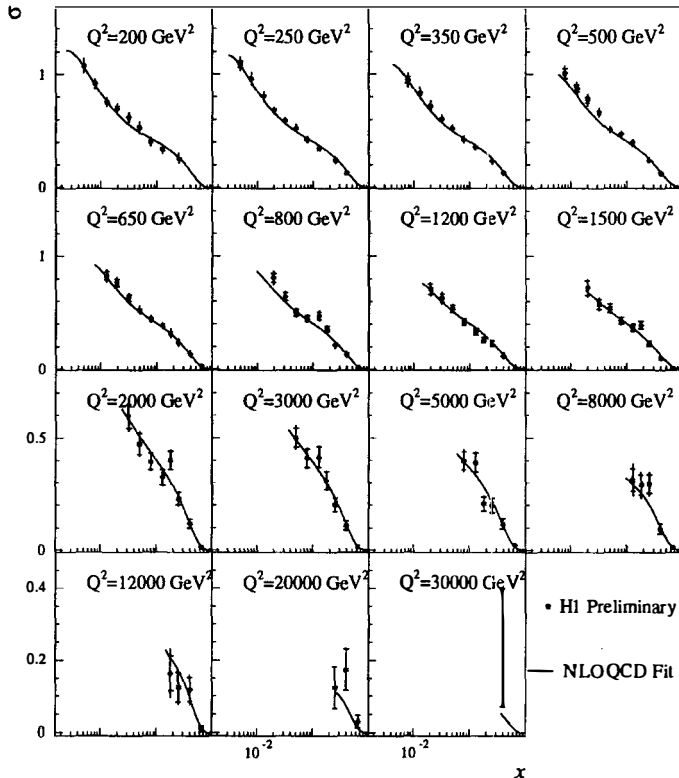


Figure 6: Double differential cross section divided by a kinematic factor $\kappa = (2\pi\alpha^2 Y_+)/(Q^4 x)$ in different Q^2 bins as a function of x . The full error bars represent the statistical and systematic errors added in quadrature. The curves represent the result of a NLO QCD fit to H1, NMC and BCDMS data.

A new measurement of the DIS cross section at high $Q^2 \geq 200 \text{ GeV}^2$ based on a luminosity of about 37 pb^{-1} is presented in Figure 6. With respect to the previous publication² the measured range is extended towards higher $5000 < Q^2 \leq 30000 \text{ GeV}^2$ and towards larger $x \leq 0.65$.

A special QCD analysis of this data has been performed. Unlike in the fit described in Section 5.2, the fit was performed to the DIS cross section directly. The charm and bottom quarks were treated as massless. The starting scale of the QCD evolution and minimum Q^2 of the data points included in this analysis were taken to be 4 GeV^2 .

Two distinct fits have been performed. One used low $Q^2 \leq 120$ GeV^2 F_2 data of H1, NMC and BCDMS only. The second fit was done including the new high Q^2 DIS cross section data. Both fits agreed within a few percent i.e. the high Q^2 measurement is reliably predicted using perturbative QCD fit based on data fixed at $Q^2 \leq 120$ GeV^2 .

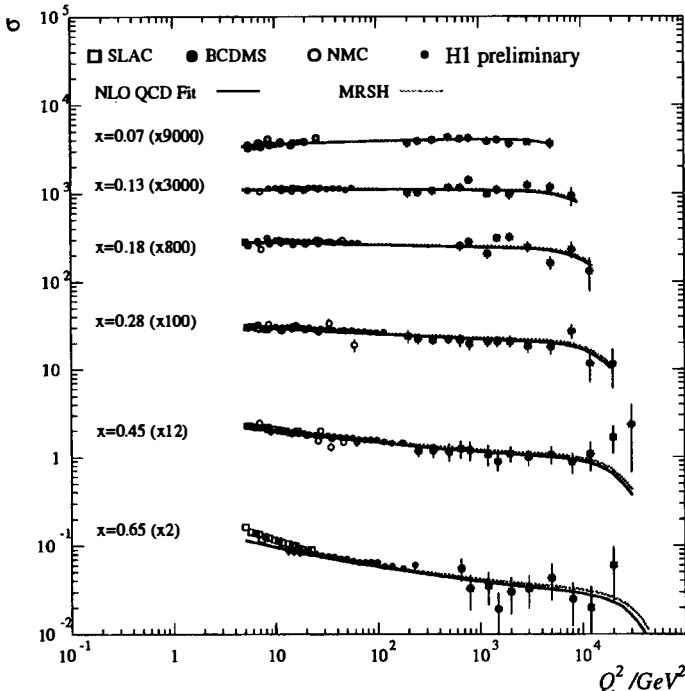


Figure 7: Double differential cross section divided by a kinematic factor $\kappa = (2\pi\alpha^2 Y_+)/ (Q^4 x)$ as a function of Q^2 for different x values measured at high x . The curves represent the results of the QCD fit (see text) and a calculation based on the MRSW parameterisations of the parton densities.

Figure 7 represents the high x part of the H1 cross section measurement together with data of fixed target experiments as a function of Q^2 . The lines show the QCD fit and calculations according to MRSW²⁶ parton densities. Up to $Q^2 \leq 10000$ GeV^2 the cross section is dominated by $F_2(x, Q^2)$. The decrease of the cross section at high x with increasing Q^2 corresponds therefore to the F_2 evolution as it is characteristic for the valence quark region $x > 0.3$.

At even higher $Q^2 > 10000$ GeV^2 the influence of the Z^0 exchange gives rise to a large contribution of the structure function $x F_3(x, Q^2)$. As the result the DIS cross section section gets smaller. In general one can see that data follows this trend, apart from the bin at $x = 0.45$ where the data points are higher than the prediction by about twice the total errors.

Based on data with 14.2 pb^{-1} of luminosity, collected in years 1994-1996, the H1 collaboration reported an excess of events⁶ at very high Q^2 . For $Q^2 > 15000$ GeV^2 , $N_{\text{obs}} = 12$ neutral current candidate events were observed where the expectation was $N_{\text{DIS}} = 4.71 \pm 0.76$ events. The probability $P(N \geq N_{\text{obs}})$ that the DIS model signal N fluctuates to $N \geq N_{\text{obs}}$ in a random set of experiments was found to be equal to 6×10^{-3} . With about 23 pb^{-1} of 1997 data added, the significance of this excess decreases: $N_{\text{obs}} = 22$ are found with $N_{\text{DIS}} = 14.8 \pm 2.13$ expected

which corresponds to a probability $\mathcal{P}(N \geq N_{\text{obs}}) = 5.9\%$

7 Conclusions

New measurements of the DIS cross section performed by the H1 collaboration extended the experimentally accessible kinematic range towards high y and high Q^2 . In the region of overlap the new data agrees with previously published results. The new data has a large sensitivity to the structure functions F_L (at low Q^2 , high y) and xF_3 (at high Q^2 and high y). In general the H1 results are in remarkable agreement with the NLO QCD analysis at $Q^2 < 15000$ GeV 2 . Some possible deviations are seen at high y where the cross section tends to be lower than expected which can be interpreted as F_L to be about 1.5 times larger than in the QCD calculation. Above $Q^2 > 15000$ GeV 2 a slight excess of the number of observed events with respect to the standard model is present at the level of 2 standard deviations.

References

1. H1 Collaboration, T. Ahmed et al., *Nucl. Phys. B* 439 (1995) 471.
2. H1 Collaboration, S. Aid et al., *Nucl. Phys. B* 470 (1996) 3.
3. ZEUS Collaboration; M. Derrick et al., *Z. Phys. C* 69 (1996) 607.
4. ZEUS Collaboration, M. Derrick et al. *Z. Phys. C* 72 (1996) 399.
5. H1 Collaboration, C. Adloff et al., *Phys. Lett. B* 393 (1997) 452.
6. H1 Collaboration, C. Adloff et al., *Z. Phys. C* 74 (1997) 191.
7. ZEUS Collaboration; J. Breitweg et al., *Z. Phys. C* 74 (1997) 207.
8. H1 Collaboration, paper submitted to EPS Conf., N-260, Jerusalem (1997).
9. H1 Collab., I. Abt et al., *Nucl. Instrum. Methods A* 386 (1997) 310 and A 386 (1997) 348.
10. G.A. Schuler and H. Spiesberger, Proceedings of the Workshop Physics at HERA, vol. 3, eds. W. Buchmüller, G. Ingelman, DESY (1992) 1419.
11. R. Engel and J. Ranft, *Phys. Rev. D* 54 (1996) 4244.
12. A. Meyer Ph.D. Thesis, Hamburg University, 1997.
13. A. Glazov Ph.D. Thesis, Humboldt University of Berlin, 1998.
14. P. Bruel, Moriond Electroweak-98.
15. H1 Collaboration, C. Adloff et al., *Nucl. Phys. B* 497 (1997) 3.
16. NMC Collaboration, M. Arneodo et al., *Nucl. Phys. B* 483 (1997) 3.
17. Yu.L. Dokshitzer, *Sov. Phys. JETP* 46 (1977) 641;
V.N. Gribov and L.N. Lipatov, *Sov. J. Nucl. Phys.* 15 (1972) 438 and 675;
G. Altarelli and G. Parisi, *Nucl. Phys. B* 126 (1977) 298.
18. M. Glück, E. Reya and A. Vogt, *Z. Phys. C* 67 (1995) 433.
19. E.B. Zijlstra and W. van Neerven, *Nucl. Phys. B* 383 (1992) 525;
S.A. Larin and J.A.M. Vermaasen, *Z. Phys. C* 57 (1993) 93.
20. E. Laenen et al., *Nucl. Phys. B* 392 (1993) 162.
21. C. Pascaud and F. Zomer, LAL preprint LAL/94-42.
22. BCDMS Collaboration, A.C. Benvenuti et al., *Phys. Lett. B* 223 (1989) 485;
CERN preprint CERN-EP/89-06.
23. ZEUS Collaboration, paper submitted to EPS Conf., N-647, Jerusalem (1997).
24. W. Vogelsang and A. Vogt, DESY preprint 95-096(1995).
25. A.D. Martin, R.G. Roberts and W.J. Stirling, *Phys. Lett. B* 387 (1996) 419.
26. A.D. Martin, R.G. Roberts and W.J. Stirling, Duram Univ. preprint DTP-93-86.